ELASTIC SCATTERING OF 27.5 MeV ALPHA PARTICLES ON ^{27}Al, ^{28}Si, ^{32}S, Ti and ^{59}Co NUCLEI AND THE r_0 DISCRETE AMBIGUITY OF THE OPTICAL POTENTIAL

By A. Bobrowska*, A. Budzanowski**, K. Grotowski*, L. Jarczyk*, B. Kamys*, S. Micek*, M. Polok*, A. Strzałkowski* and Z. Wróbel*

Institute of Physics, Jagellonian University, Cracow*

and

Institute of Nuclear Physics, Cracow**

(Received December 6, 1971; Revised paper received March 8, 1972)

Angular distributions for elastic scattering of alpha particles on ^{27}Al, ^{28}Si, ^{32}S, Ti and ^{59}Co nuclei have been measured in the angular range from about 20° to 179° (LAB). The experimental data were fitted with the optical model in full angular range. Many sets of four-parameter potentials, describing the elastic scattering, were found with the depths of the real part ranging from 40 to 450 MeV. A new discrete ambiguity in the optical model namely in r_0 was observed.

1. Introduction

The elastic scattering of nuclear particles is generally well described in terms of the optical model of the interaction. In the case of scattering of nucleons unambiguous sets of optical model parameters can be found giving very satisfactory fits to experimental data. The dependence of these parameters on the energy of bombarding nucleons, on the neutron excess $N-Z$ and coulomb factor $\frac{Z}{\sqrt[3]{A}}$ can also be determined and understood on the basis of the microscopic description [1, 2]. In spite of this, scattering of alpha particles is far form understanding. Most measurements of the elastic scattering of alpha particles have been performed in the angular range up to 120°, not too many of them overstep 170°. The results of the phenomenological optical model analysis of alpha elastic scattering data made so far by different authors is rather inconclusive and not very successful [3].

* Address: Instytut Fizyki, Uniwersytet Jagielloński, Kraków 16, Reymonta 4, Poland.
** Address: Instytut Fizyki Jądrowej, Kraków 23, Radzikowskiego 152, Poland.

The aim of this work was a systematic study of various existing ambiguities in a simple 4-parameter optical model description based on experimental data taken for different nuclides in a wide range of scattering angles.

Measurements have been made for elastic scattering of 27.5 MeV alpha particles on ^{27}Al, ^{28}Si, ^{32}S, Ti and ^{59}Co nuclei and for region of C M angles up to 179°.

2. *Experimental arrangement*

The experiment was carried out with the alpha particle beam of the 120 cm cyclotron of the Institute of Nuclear Physics in Cracow. The lay-out of the beam line is presented in Fig. 1. Two quadrupole lenses focused the beam on target located at the distance of about 12 m from the cyclotron in the centre of a scattering chamber. Two system of crossed

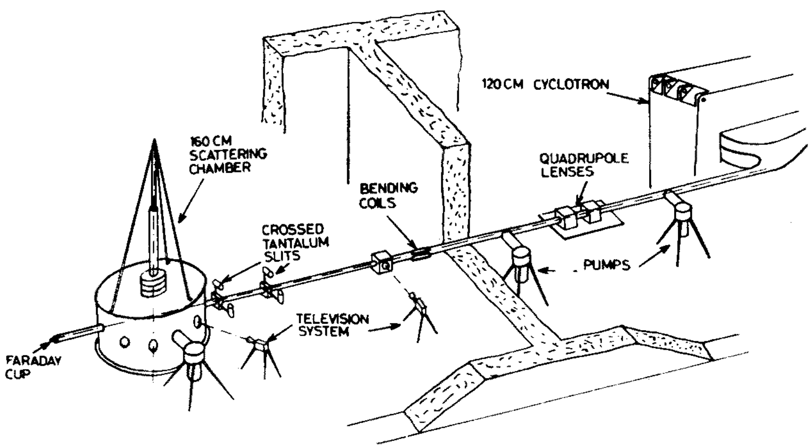

Fig. 1. The lay-out of the beam line

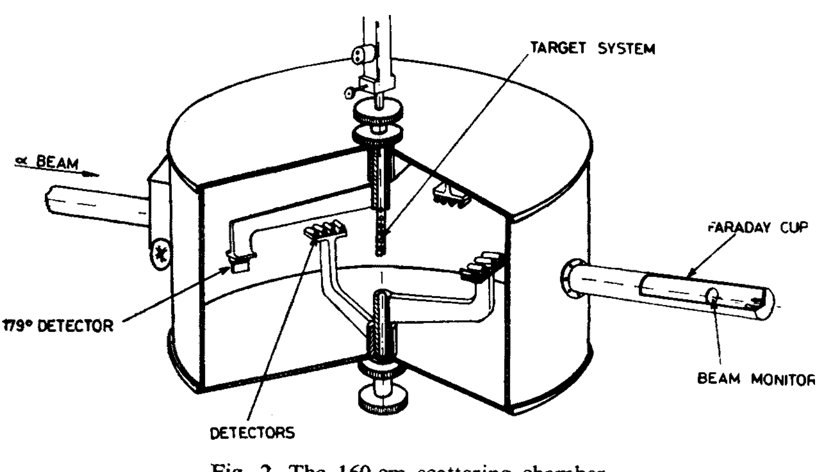

Fig. 2. The 160 cm scattering chamber

tantalum slits were used in order to get a good collimation of the beam on 3×3 mm^2 spot on the target. The position of these slits could be adjusted by the remote control. Two pairs of the deflection coils mounted on the beam tube could shift the beam in the right-left as well as in the up-down directions. The spread of the beam and its location was observed in several points along the beam line by means of the closed circuit television system. After passing the collimating system the angular spread of the beam was less than 0.4° FWHM.

Measurements of angular distributions were performed with the large scattering chamber of 160 cm diameter and 80 cm height. The details of the chamber are presented in Fig. 2. Thirteen semiconductor detectors mounted on four rotatable arms were used for detection of scattered particles. Angular position of each arm could be measured with the accuracy of 0.1 degree. Particles scattered at extreme backward angles up to 179° were detected by means of a special very narrow counter. Each detector was mounted on a small supporting table. Its orientation was optically adjusted with great accuracy. Angular resolution of the back scattering counter was about $\pm 0.1°$ while for the others was $\pm 0.5°$. Seven different targets could be inserted into the beam from an external vacuum store through a vacuum lock. A special arrangement was provided to prepare targets by evaporation inside of the vacuum store. The diameter of the target was about 30 mm. Surface densities of these targets were determined in the usual way by weighing and measuring the area. During the cross-section measurements the thickness of the target was checked by a special semidonductor monitor viewing the target at a fixed angle of about 30° (LAB).

The energy of the incident beam was measured by means of the differential absorption method. The energy measuring device was mounted on a separate beam line. An aluminium absorber of variable thickness was placed in front of the Faraday cup. Currents of alpha particles captured in the aluminium absorber and those collected in the Faraday cup were compared together by means of a differential DC amplifier. The absorber of the variable thickness was made in form of two foil holders which could be shifted independently by a remote control. Each holder contained 10 absorbers of different thicknesses. In this way the energy of alpha particles could be measured in 50 keV steps.

In order to avoid spurious currents caused by secondary electrons the region of aluminium absorber and of the entrance of the Faraday cup was kept in a strong magnetic field. The absolute reliability of this measurement was checked by the kinematic method and by comparison with the well known energy of alpha particles from minute activity of the Bi isotope. The accuracy of the absolute energy measurement was ± 100 keV.

The intensity of the alpha-particle beam was monitored in two independent ways in order to ensure the proper normalization of the cross-section. The total charge in the Faraday cup was measured by a standart current integrator. The Faraday cup was aquiped with a system of baffles in order to avoid back scattering from the beam stopper what could affect measurements at extremely large angles. The distance between the beam stopper and the centre of scattering chamber was 225 cm. In addition the beam intensity was monitored by two semiconductor detectors counting alpha particles scattered from a gold foil placed in the beam in front of the Faraday cup. The intensity of the beam was proportional to the sum of counting rates of both counters whereas the ratio of both counting rates indicates the possible change of the beam spot position on the target.

Silicon surface barrier counters with the thickness of the depletion layer of 0.5 mm were used in this experiment. The detectors were made in the Department of Physical Electronics of the Institute of Physics of the Jagellonian University. The pulses from counters were sent through charge sensitive amplifiers to three 512 channel analysers. A special memory splitting coding system was used enabling simultaneous use of 13 counters.

3. Experimental procedure and results

The solid angle of each detector was evaluated from geometry and rechecked by measuring Rutherford scattering from a gold target. The zero of the angular scale was precisely determined as the position of the symmetry line for the left-right Rutherford scattering.

TABLE I

Target	Method of preparation	Thickness mg/cm^2	Error of the absolute value of the cross-section %
Al	evaporated	1.05	5.2
Si	SiO_2 blowed	0.542	7.5
S	evaporated on C backing	2.64	8.7
Ti	evaporated	0.244	9.7
Co	rolled	1.81	11.1

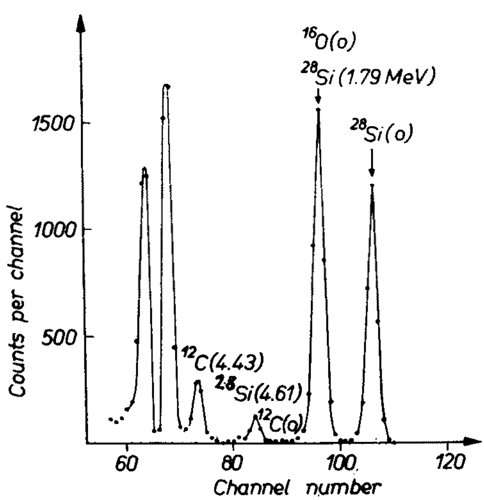

Fig. 3

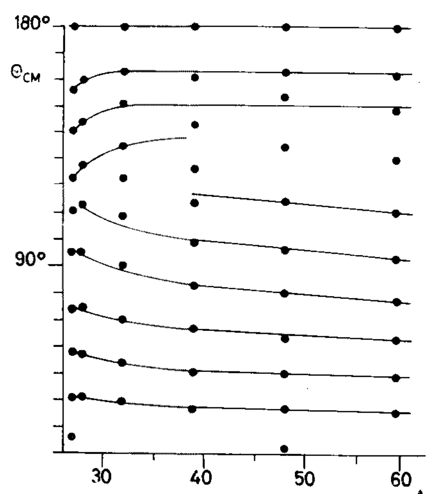

Fig. 4

Fig. 3. Alpha-particle spectrum for the Si target at 47.5° scattering angle

Fig. 4. The CM angles corresponding to the maxima of the differential cross-section *versus* the mass number of target nuclei

The positions of antiscattering baffles at the entrance to the Faraday cup were optimised in order to diminish the background for extreme backward scattering angles.

The angular distributions of alpha-particles were measured in the angular range from about 20° up to 177.5° in 2.5° intervals in the LAB system and at 178° and 179° (LAB). Measurements were performed for ^{27}Al, ^{28}Si, ^{32}S, Ti and ^{59}Co nuclei at alpha particle energy 27.5 MeV. The methods of preparation and thicknesses of targets are presented in Table I.

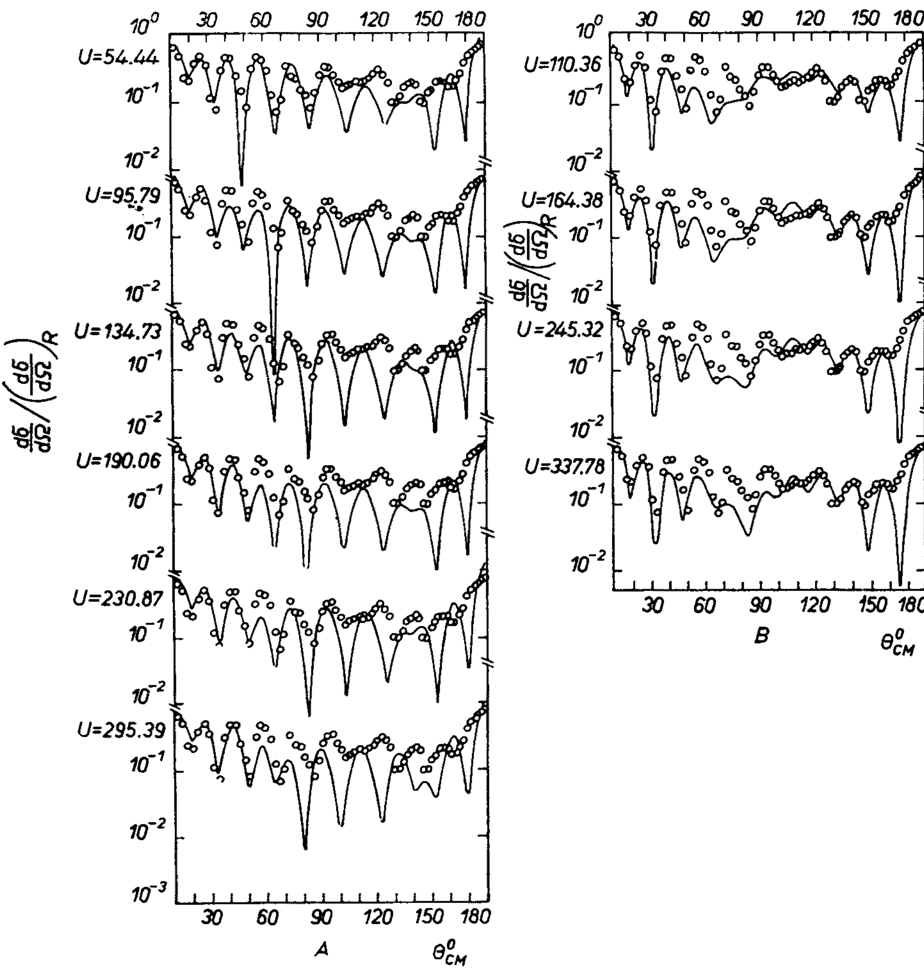

Fig. 5a

In order to reduce errors in absolute value of cross-section three independent measurements using three different targets for each element were carried out. Fig. 3 shows a typical spectrum obtained for Si target at 47.5° scattering angle. The overall energy resolution including the beam energy spread was estimated to be of about 250 keV FWHM.

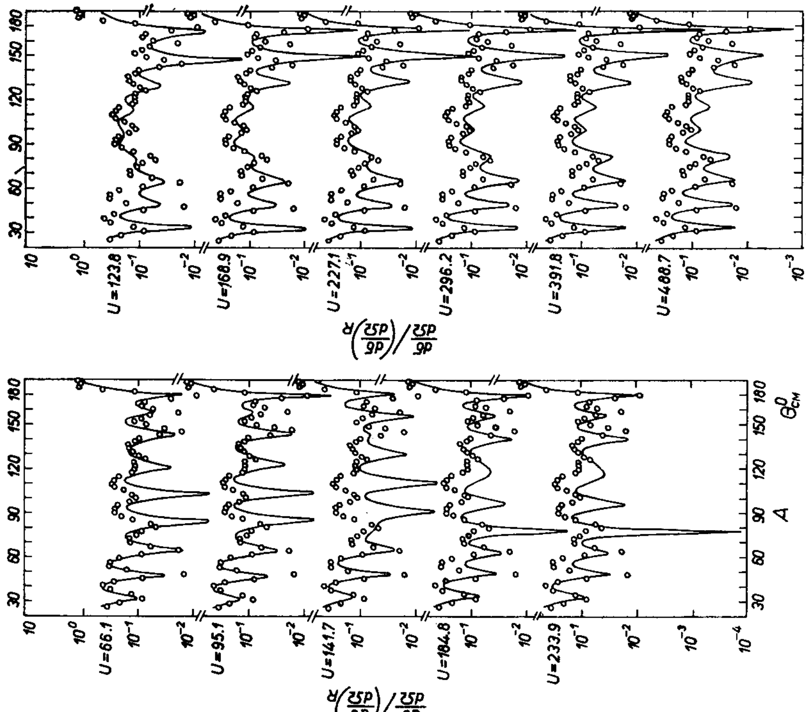
U=123.8
U=168.9
U=227.1
U=296.2
U=391.8
U=488.7
B
U=66.1
U=95.1
U=141.7
U=184.8
U=233.9
A
Θ^0_{CM}

Fig. 5c

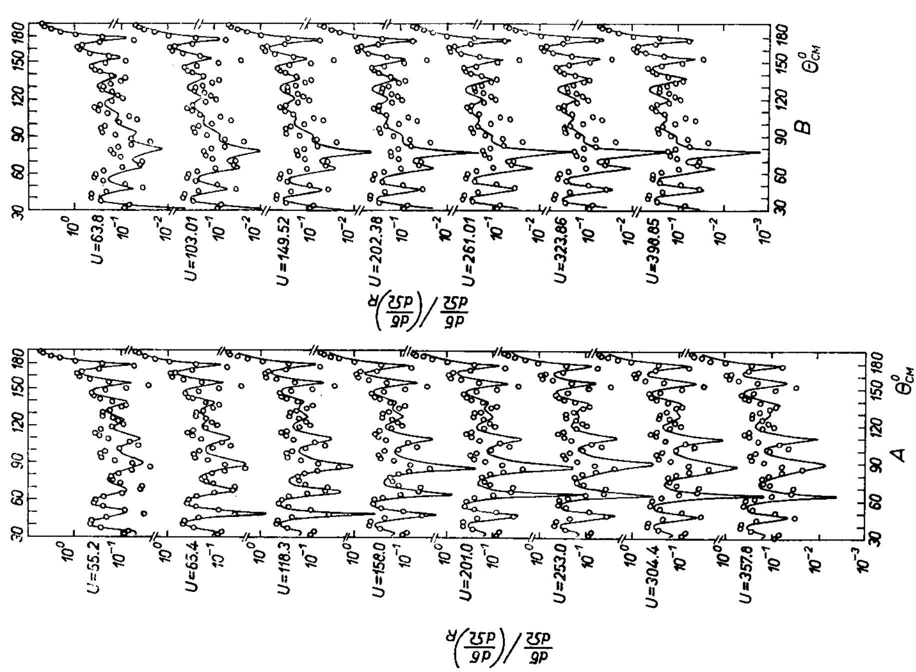
U=63.8
U=103.01
U=149.52
U=202.38
U=261.01
U=323.86
U=398.85
B
U=55.2
U=65.4
U=118.3
U=158.0
U=201.0
U=253.0
U=304.4
U=357.8
A
Θ^0_{CM}

Fig. 5b

The experimental angular distributions are presented in Figs 5. The ralative errors in the values of the experimental differential cross-section vary from 1% to 10% in deep minima. The errors of absolute values of cross-section are given in Table I.

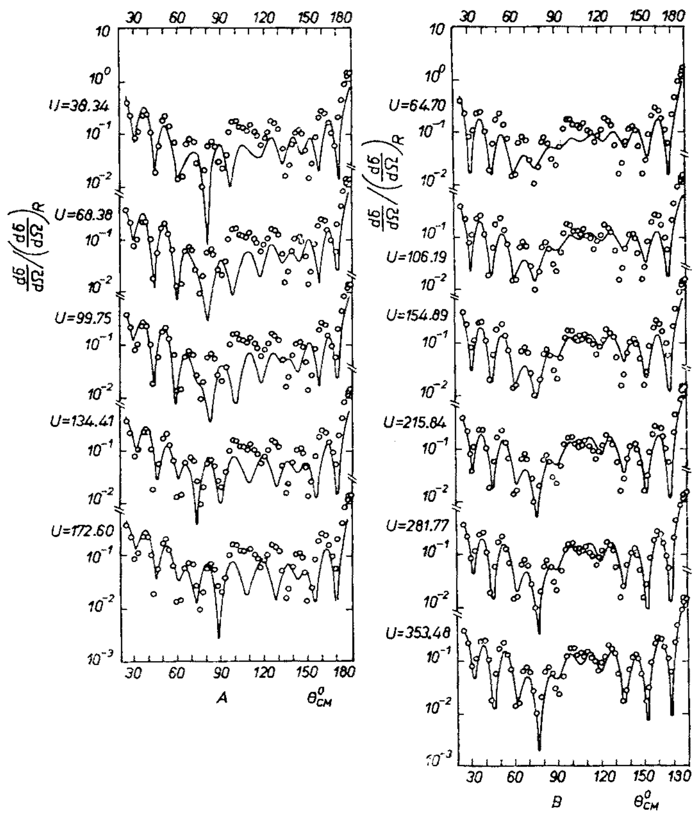

Fig. 5d

Numerical results including relative errors of individual measurements are available in Report 624/PL of the Institute of Nuclear Physics in Cracow.

Angular distribution of alpha particles exhibit a pronounced diffraction pattern. The C M angles corresponding to the maxima of the differential cross-section *versus* the

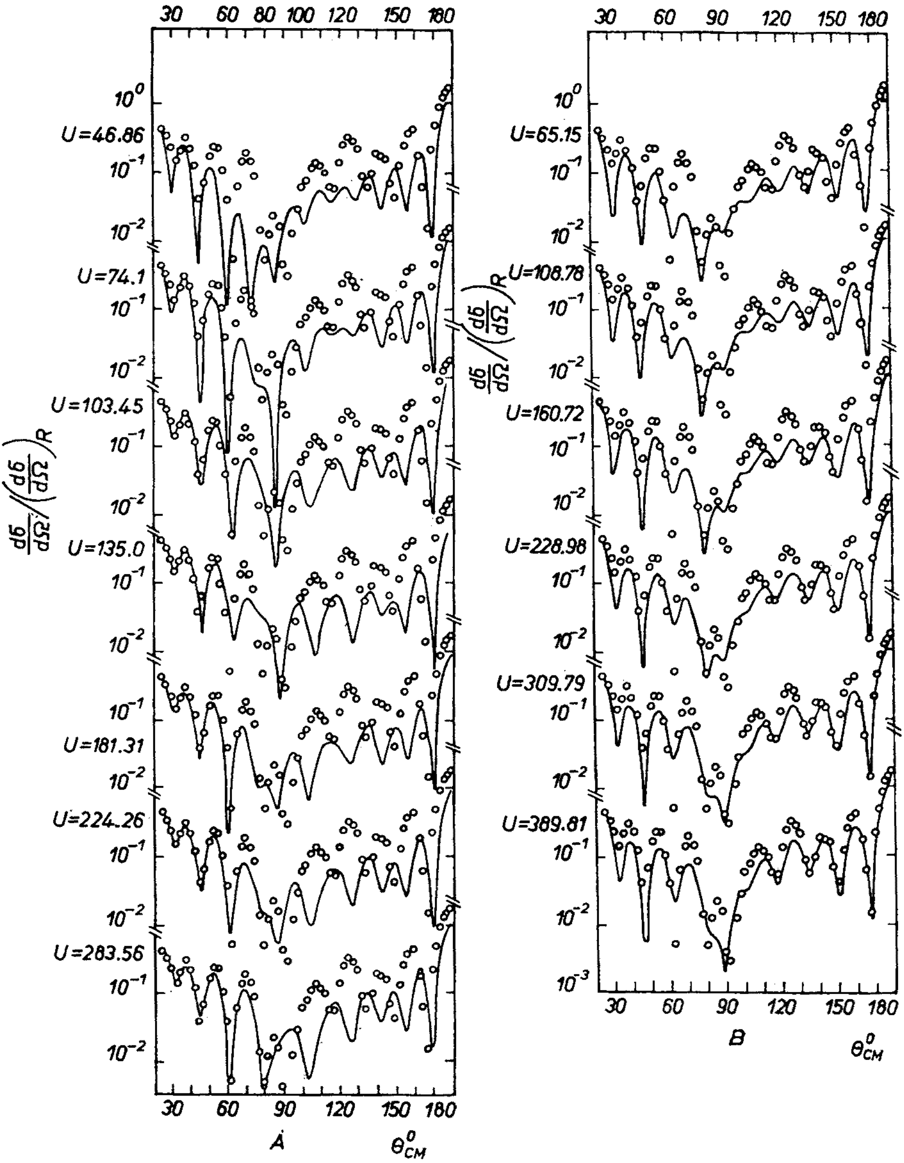

Fig. 5e

mass number of target nuclei are presented in Fig. 4. In forward scattering region diffraction pattern shifts towards smaller angles with increasing mass number according to the prediction of the simple diffraction model of scattering.

In the backward scattering region three distinct maxima can be noticed for all observed nuclei. This region of scattering can be described by a simple glory scattering model [4].

For some nuclei as ^{28}Si and ^{32}S the backward scattering cross-section is strongly enhanced. Similar effect has been previously observed for ^{12}C [5], ^{16}O [6], ^{24}Mg [7], ^{39}K [8, 9] and ^{40}Ca [10, 11]. With the excption of ^{39}K all of them are "alpha nuclei".

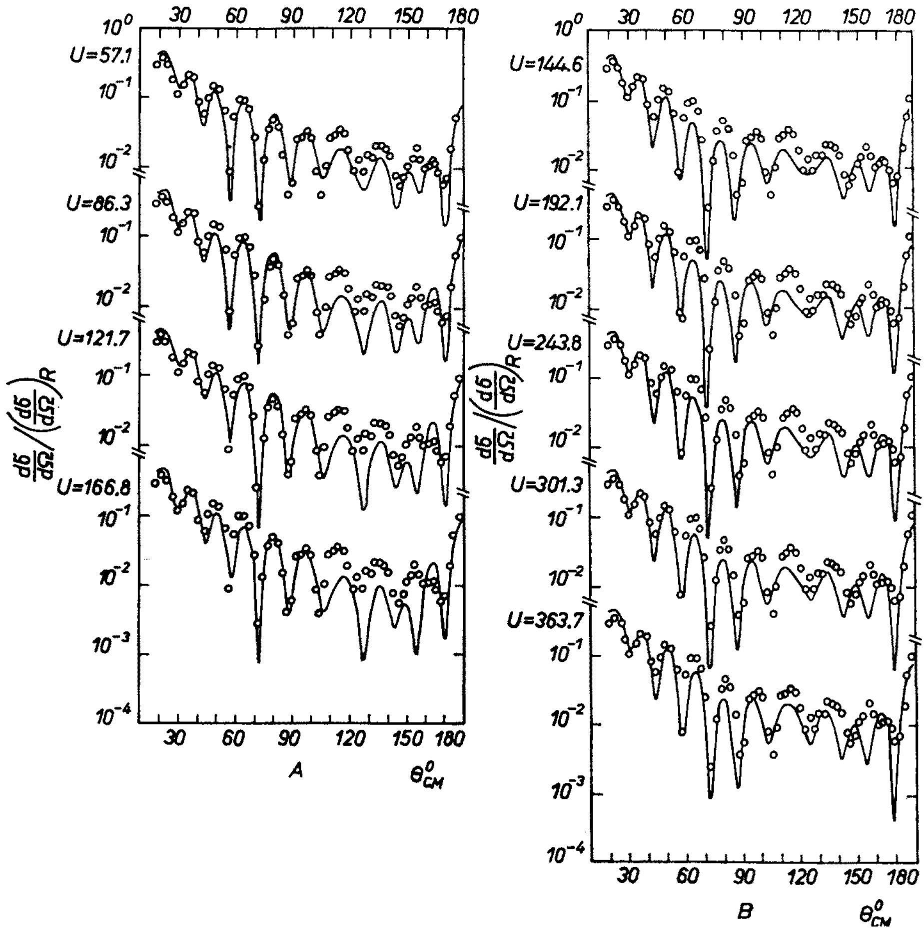

Fig. 5f

For Ti and ^{59}Co nuclei the average cross-section drops down with the angle to the value of about 10^{-2} of the Rutherford cross-section. Nevertheless they show a well pronounced glory maximum at 180°.

In case of ^{27}Al the backward scattering cross-section is enhanced when compared with Ti or ^{59}Co but the oscillations of the cross-section are less pronounced. This effect may be connected with the coupling of the target spin and the angular momentum of relative motion.

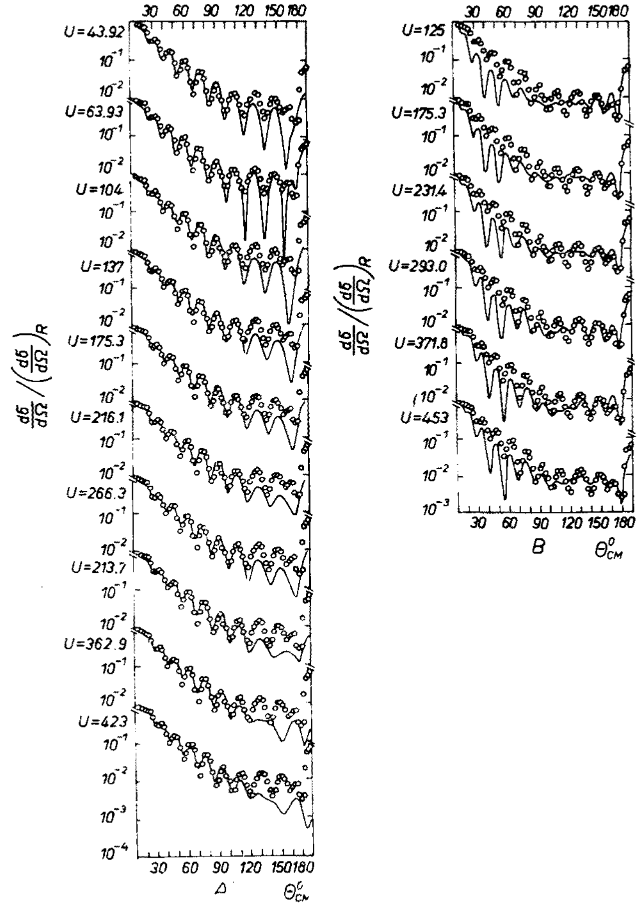

Fig. 5g

Fig. 5. Differential cross-section of the elastic scattering of alpha particles on the ^{27}Al, ^{28}Si, ^{32}S, ^{39}K, ^{40}Ca and ^{59}Co nuclei. Experimental data are indicated by circles, the continuous lines indicate the optical model fits. A — fits with larger radius parameter, B — fits with smaller radius parameter

4. Optical model analysis

The optical model analysis has been performed using the automatic search programmes ALA-1 [12] and MARYLKA-1 written for the GIER computer and ODRA 1204 computer. The interaction of alpha particles with nuclei was described by a complex potential of the form:

$$V(r) = U_c(r)+(U+iW)f(r)$$

where $U_c(r)$ is the Coulomb potential due to the uniformly charged sphere of the radius $1.34\ A^{1/3}$, U and W indicate the real and imaginary depths parameters and A is the mass number of the target nucleus. The radial form-factor has the usual Saxon-Woods form

$$f(r) = \frac{1}{1+\exp \frac{r-r_0 \sqrt[3]{A}}{a}}$$

with half-way radius $r_0 \sqrt[3]{A}$ and diffuseness a.

The best fit optical model parameters were found by minimizing the quantity

$$\chi^2 = \frac{1}{N} \sum_{i=1}^{N} \left(\frac{\sigma^t(\theta i) - \sigma^{\exp}(\theta i)}{\Delta\sigma^{\exp}(\theta i)} \right)^2$$

where $\sigma^{\exp}(\theta i)$ and $\sigma^t(\theta i)$ are the experimental and theoretical values of the differential cross-section at the angle θ, and the summation runs over all N measured points, $\Delta\sigma^{\exp}(\theta_i)$ denotes the error of the corresponding experimental value. In the first step of the analysis the approximate location of minima of χ^2 value in the four parameter (U, W, r_0, a) space was investigated. In order to assure that all local minima of χ^2 will be found the automatic search was carried out in the (W, a) subspace, while U and r_0 were taken from the following grid:

$$40 \text{ MeV} \leqslant U \leqslant 450 \text{ MeV} \qquad \Delta U = 10 \text{ MeV}$$

$$0.8 \text{ fm} \leqslant r_0 \leqslant 2 \text{ fm} \qquad \Delta r_0 = 0.1 \text{ fm}.$$

In the second step all sets of parameters corresponding to local minima found in this way were used as starting parameters for the four parameter search.

The obtained results are presented in tables II–VIII and best fits are shown in Fig. 5. The results for ^{39}K and ^{40}Ca obtained previously [8, 10] were also included in the analysis.

TABLE II

The optical potential parameters for ^{27}Al

No	U MeV	W MeV	r_0 fm	a fm	n	σ_A mb	χ^2/N
A1	54.44	10.01	1.729	0.455	6	1180	660
A2	95.79	14.57	1.655	0.443	7	1177	840
A3	134.73	17.07	1.642	0.413	8	1170	880
A4	190.06	21.68	1.565	0.440	9	1183	900
A5	230.87	21.77	1.584	0.405	10	1171	850
A6	295.39	26.10	1.563	0.411	11	1198	980
B1	110.36	18.55	1.276	0.790	7	1258	490
B2	164.38	22.15	1.229	0.746	8	1251	510
B3	245.32	28.83	1.144	0.738	9	1248	570
B4	337.78	35.287	1.089	0.725	10	1249	620

TABLE III

The optical potential parameters for ^{28}Si

No	U MeV	W MeV	r_0 fm	a fm	n	σ_A mb	χ^2/N
A1	55.16	8.52	1.629	0.576	7	1199	270
A2	85.42	10.42	1.620	0.498	8	1194	350
A3	118.29	12.58	1.648	0.483	9	1218	440
A4	158.03	15.01	1.632	0.446	10	1237	480
A5	201.03	17.31	1.619	0.439	11	1254	520
A6	253.00	20.16	1.583	0.437	12	1247	540
A7	304.38	22.54	1.588	0.426	13	1263	580
A8	357.75	24.48	1.586	0.413	14	1262	620
B1	63.81	12.81	1.444	0.800	7	1310	450
B2	103.01	15.39	1.384	0.736	8	1282	430
B3	149.52	18.03	1.346	0.698	9	1278	420
B4	202.38	20.55	1.314	0.673	10	1279	400
B5	261.01	23.13	1.293	0.647	11	1276	390
B6	323.86	25.58	1.287	0.626	12	1283	360
B7	398.85	28.26	1.269	0.617	13	1295	350

TABLE IV

The optical potential parameters for ^{32}S

No	U MeV	W MeV	r_0 fm	a fm	n	σ_A mb	χ^2/N
A1	66.12	9.03	1.817	0.409	8	1321	280
A2	95.08	11.07	1.790	0.388	9	1314	400
A3	141.68	16.76	1.629	0.436	10	1251	660
A4	184.81	19.53	1.521	0.482	11	1237	500
A5	233.85	22.22	1.506	0.474	12	1246	510
B1	123.80	19.06	1.079	0.892	8	1200	600
B2	168.92	22.41	1.110	0.795	9	1194	570
B3	227.12	26.64	1.101	0.744	10	1190	590
B4	296.23	31.25	1.083	0.708	11	1180	620
B5	391.78	37.60	1.038	0.697	12	1178	660
B6	488.70	43.67	1.014	0.680	13	1174	710

TABLE V

The optical parameters for ^{39}K

No	U MeV	W MeV	r_0 fm	a fm	n	σ_A mb	χ^2/N
A1	38.34	7.32	1.795	0.534	6	1448	500
A2	68.38	10.16	1.692	0.525	7	1415	610
A3	99.75	12.73	1.639	0.516	8	1407	650
A4	134.41	16.00	1.528	0.510	9	1299	490
A5	172.60	18.13	1.526	0.486	10	1304	560
B1	64.70	14.41	1.280	0.909	6	1348	430
B2	106.19	16.48	1.214	0.845	7	1308	310
B3	154.89	19.16	1.165	0.806	8	1295	240
B4	215.84	22.25	1.111	0.785	9	1287	200
B5	281.77	25.65	1.082	0.761	10	1282	160
B6	353.84	28.98	1.063	0.737	11	1279	140

TABLE VI

The optical potential parameters for ^{40}Ca

No	U MeV	W MeV	r_0 fm	a fm	n	σ_A mb	χ^2/N
A1	46.86	9.12	1.614	0.719	6	1415	3670
A2	74.10	10.89	1.580	0.624	7	1397	3480
A3	103.45	12.26	1.560	0.528	8	1295	3990
A4	135.00	15.00	1.550	0.500	9	1294	4160
A5	181.31	18.00	1.504	0.543	10	1370	3550
A6	224.26	19.75	1.488	0.516	11	1342	3530
A7	283.56	21.77	1.446	0.509	12	1315	3500
B1	65.15	12.23	1.281	0.862	6	1247	1300
B2	108.78	16.00	1.200	0.834	7	1250	1200
B3	160.72	20.15	1.135	0.800	8	1239	970
B4	228.98	24.36	1.066	0.790	9	1233	880
B5	309.79	28.41	1.013	0.778	10	1228	720
B6	389.81	31.97	0.991	0.758	11	1229	580

TABLE VII

The optical potential parameters for Ti

No	U MeV	W MeV	r_0 fm	a fm	n	σA mb	χ^2/N
A1	57.09	12.22	1.556	0.590	8	1369	170
A2	86.30	14.37	1.511	0.573	9	1370	190
A3	121.73	17.35	1.467	0.558	10	1357	230
A4	166.77	21.07	1.407	0.566	11	1351	260
B1	144.57	22.06	1.381	0.615	10	1370	260
B2	192.11	25.78	1.337	0.614	11	1363	250
B3	234.82	29.12	1.360	0.606	12	1363	240
B4	301.32	32.44	1.279	0.599	13	1360	240
B5	363.73	35.56	1.256	0.593	14	1356	230

TABLE VIII

The optical potential parameters for ^{59}Co

No	U MeV	W MeV	r_0 fm	a fm	n	σ_A mb	χ^2/N
A1	43.92	11.62	1.633	0.493	7	1367	160
A2	63.93	11.01	1.643	0.486	8	1441	160
A3	104.58	19.17	1.519	0.489	9	1340	190
A4	137.57	22.75	1.487	0.485	10	1334	190
A5	175.34	26.02	1.458	0.484	11	1332	200
A6	216.10	29.03	1.433	0.482	12	1330	200
A7	266.29	32.74	1.406	0.482	13	1326	210
A8	313.72	36.58	1.388	0.481	14	1326	210
A9	362.88	40.41	1.370	0.481	15	1327	210
A10	423.20	46.26	1.350	0.481	16	1323	210
B1	125.22	25.76	1.062	1.018	8	1544	810
B2	175.29	30.97	1.019	0.968	9	1504	720
B3	231.39	36.05	0.990	0.927	10	1478	660
B4	293.00	40.22	0.968	0.893	11	1439	600
B5	371.76	46.23	0.933	0.835	12	1428	570
B6	453.02	52.00	0.916	0.850	13	1428	550

5. *Discussion*

For each of analysed nuclei nine to sixteen sets of optical potential parameters were found in the investigated region. Two groups of potential parameters could be clearly distinguished corresponding to the smaller and larger values of raadius parameter r_0. These two groups of parameters are marked in Fig. 5 and Tables II–VIII A for the larger

r_0 values an B for the smaller ones. As can be seen the potentials of the group A give better description of experimental data in the forward angular range (up to 90°) while those of the group B better reproduce cross-sections in the backward scattering region. In case of ^{39}K and ^{40}Ca nuclei the parameters of the group B give better fits in full angular

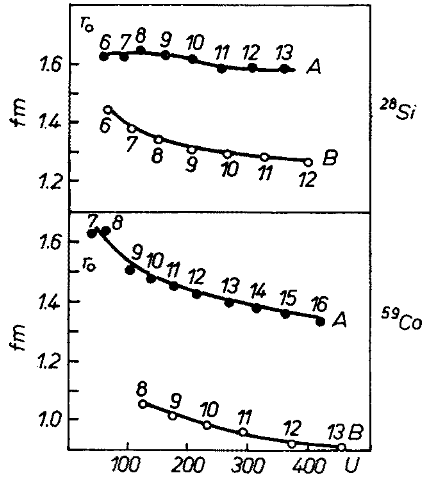

Fig. 6. Locations of local minima of χ^2 in the (U, r_0) plane for ^{28}Si and ^{59}Co

region. Fitting separately the forward or backward angular region only the parameters with large or small radius respectively were obtained.

In Fig. 6 locations of local minima of χ^2 in the (U, r_0) plane are presented for ^{28}Si and ^{59}Co. The points corresponding to the parameters of the type A or B are connected by lines.

Different optical potentials generate radial wave functions with different number of nodes inside of the nucleus which are matched to practically the same wave functions in the asymptotic region. This numbers [n] are indicated in Fig. 6 and Tables II–VIII.

We notice that along each line A or B the number of nodes increases one by one with increasing U. This corresponds to the well known, discrete U-ambiguity illustrated by Fig. 7a.

Another kind of discrete ambiguity is clearly seen from Fig. 6. Minima of χ^2 on lines A and B are placed at nearly the same values of U. Each of so conjugated potentials generates radial wave functions differing by one or two in number of nodes. This kind of radial discrete ambiguity is illustrated by Fig. 7b.

Most of so far performed optical model analysis for alpha-particles started from radius of interaction equal to the sum of radii for alpha particles R and target nucleus R_t in consequence leading to the group A of parameters. However, in some analysis performed for ^{39}K and ^{40}Ca nuclei the applicability of potentials of the group B was also shown [13]. The microscopic optical model for alpha particles sheds light on this problem. According to recent calculations in which the real part of the potential was obtained by double folding procedure the small value of r_0 is evidently favorized [14]. In the microscopic approach the real part of the potential is given by an overlap of the effective nucleon--nucleon interaction and both alpha-particle and target nucleus density distributions. The half value of the real potential depth is reached when an alpha-particle penetrates half a way into target nucleus. In consequence the interaction radius equals approximately to the half-way radius of the density distribution of the target nucleus (R_T).

It is interesting to notice that the potential with the real part obtained by double folding procedure gives in general better fits to experimental data than similar potential

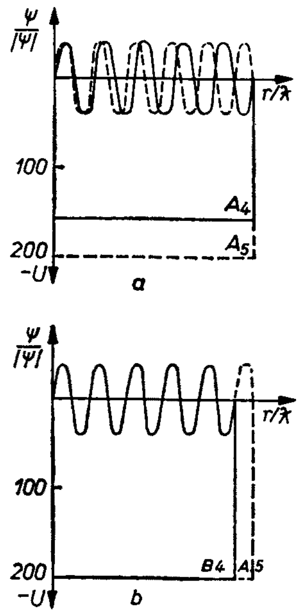

Fig. 7a, b. The phase of the radial part of the $l = 0$ partial wave function for the elastic scattering of 27.5 MeV alpha particles from ^{28}Si calculated for the potentials differing in depth (7a) and in radius parameters (7b)

of the group *B*. This is evidently due to differences in form factors of both potentials in the surface region. The microscopic potential is not of the Saxon-Woods shape having shorter tail. This property was confirmed by recent calculations made for elastic scattering of alpha particles in the region of Coulomb barrier [15].

As it was shown above the half-way radius of the real part of the potential should have the value $R = R_T$. However, the imaginary part of the potential can extend to larger R values reaching $R = R_\alpha + R_T$ as the reaction processes take place mainly in the surface region.

It is worthwhile to mention that for all sets of parameters *A* and *B* the value of the real part of the potential at the strong absorption radius is the same with accuracy of 10% in agreement with Ref. [16].

The authors are much indebted to the cyclotron and computer staffs for running both facilities and to Miss I. Kluska and Mrs N. Kolonko for their assistance in measurements.

REFERENCES

[1] G. W. Greenlees, G. J. Pyle, Y. C. Tang, *Phys. Rev.*, **171**, 1115 (1968).
[2] L. W. Owen, *Ph. D. Thesis* (1970).
[3] P. E. Hodgson, *Advances in Phys.*, **17**, 563 (1968).
[4] H. C. Bryant, N. Jarmie, *Ann. Phys.* (USA), **47**, 127 (1968); H. Niewodniczański, A. Strzałkowski, *Nuclear Phys.*, **A126**, 369 (1969); A. Bobrowska, A. Budzanowski, K. Grotowski, L. Jarczyk, S. Micek, H. Niewodniczański, A. Strzałkowski, Z. Wróbel, *Report INP*, No 624 /PL/ 1968.
[5] J. C. Corelli, E. Bleuler, D. J. Tendam, *Phys. Rev.*, **116**, 1184 (1959).
[6] A. A. Cowley, G. Heymann, *Nuclear Phys.*, **A146**, 465 (1970).
[7] R. H. Davis, *Symposium on Recent Progress in Nuclear Physics with Tandems*, Heidelberg 1966.
[8] A. Bobrowska, A. Budzanowski, K. Grotowski, L. Jarczyk, S. Micek, H. Niewodniczański, A. Strzałkowski, Z. Wróbel, *Nuclear Phys.*, **A126**, 361 (1969).
[9] R. J. Peterson, *Phys. Rev.*, **172**, 1112 (1968); C. R. Gruhn, N. S. Wall, *Nuclear Phys.*, **81**, 161 (1966).
[10] A. Budzanowski, K. Grotowski, L. Jarczyk, B. Łazarska, H. Niewodniczański, S. Micek, A. Strzałkowski, Z. Wróbel, *Phys. Letters*, **16**, 135 (1965).
[11] C. R. Gruhn, N. S. Wall, *Nuclear Phys.*, **81**, 161 (1966); C. P. Robinson, J. P. Aldridge, J. John, R. H. Davis, *Phys. Rev.*, **171**, 171 (1968); G. K. Gaul, P. Lüdecke, R. Santo, H. Schmeing, *Nuclear Phys.*, **A137**, 177 (1969).
[12] A. Dudek, *Report INP*, No 553 /PL/ 1967.
[13] L. Mc Fadden, G. R. Satchler, *Nuclear Phys.*, **84**, 177 (1966).
[14] D. F. Jackson, V. K. Kombhavi, *Phys. Rev.*, **178**, 1626 (1969); C. G. Morgan, D. F. Jackson, *Phys. Rev.*, **188**, 1758 (1969); D. F. Jackson, *Phys. Letters*, **32B**, 233 (1970); K. Grotowski, A. Strzałkowski, *Report INP*, No 720 /PL/ 1970.
[15] M. Grzywacz, private communication.
[16] D. F. Jackson, C. G. Morgan, *Phys. Rev.*, **175**, 1402 (1968).